Journal of Optics

Special issue
Graphene nanophotonics
A Yu Nikitin, S A Maier and L Martin-Moreno
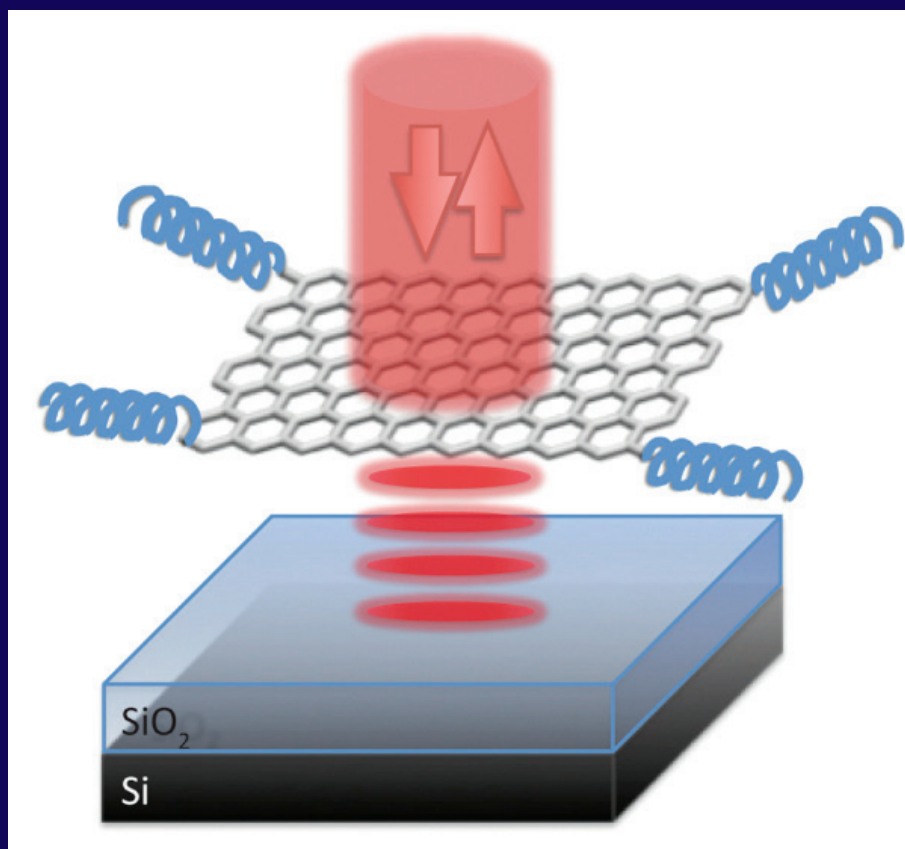
Time- and space-modulated Raman signals in graphene-based optical cavities

Antoine Reserbat-Plantey[1,4]**, Svetlana Klyatskaya**[2]**, Valérie Reita**[1]**,
Laëtitia Marty**[1]**, Olivier Arcizet**[1]**, Mario Ruben**[2,3]**, Nedjma Bendiab**[1] **and
Vincent Bouchiat**[1]

[1] Institut Néel, CNRS-UJF-INP, F-38042 Grenoble Cedex 09, France
[2] Institute of Nanotechnology, Karlsruhe Institute of Technology (KIT), Germany
[3] IPCMS-CNRS-Université de Strasbourg, F-67034 Strasbourg, France

Abstract
We present fabrication and optical characterization of micro-cavities made of multilayer
graphene (MLG) cantilevers clamped by metallic electrodes and suspended over Si/SiO$_2$
substrates. Graphene cantilevers act as semi-transparent mirrors closing air wedge optical
cavities. This simple geometry implements a standing-wave optical resonator along with a
mechanical one. Equal thickness interference fringes are observed in both Raman and
Rayleigh backscattered signals, with interfringe given by their specific wavelength. Chromatic
dispersion within the cavity makes possible the spatial modulation of graphene Raman lines
and selective rejection of the silicon background signal. Electrostatic actuation of the
multilayer graphene cantilever by a gate voltage tunes the cavity length and induces space and
time modulation of the backscattered light, including the Raman lines. We demonstrate the
potential of these systems for high-sensitivity Raman measurements of generic molecular
species grafted on a multilayer graphene surface. The Raman signal of the molecular layer can
be modulated both in time and space in a similar fashion and shows enhancement with respect
to a collapsed membrane.

(Some figures may appear in colour only in the online journal)

1. Optical properties of graphitic systems

1.1. Introduction: interaction of light with graphene

Graphitic carbon nanostructures are generally known to
produce very efficient light-absorbing media [1]. Indeed the
'blackest' materials ever manufactured are based on carbon
nanotube forests. Interestingly, the exact same carbon phases
when made very thin and flat (such as in carbon nanotube
thin films or stacked graphene layers) provide extremely
promising candidates [2] for the implementation of flexible
and transparent electrodes. This apparent paradox can be

easily explained by looking at the variety of structures and
shapes into which nanostructures based on sp^2 hybridized
carbon can be assembled down to the atomic level. Among
all these allotropes, graphene is known for providing a
flat 2D material with outstanding optical, electrical and
mechanical properties [3]. Optics in graphene has had an
historical role, as it was strongly involved in the first isolation
of a monolayer [4–6]. Indeed, a single layer of graphene
can be easily seen under an optical microscope as the
reflected light has a sufficient phase shift [7] such that it
can be detected by the naked eye. Optical methods based
on reflectometry have been identified as critical to efficiently
sort graphene multilayers (MLG) obtained by exfoliation
techniques, as it readily allows the quantitative identification
of the number of stacked layers [8]. Moreover, owing to

[4] Present address: ICFO-Institut de Ciencies Fotoniques, Mediterranean
Technology Park, 08860 Castelldefels, Barcelona, Spain.

its peculiar quantum electronic properties, graphene acts as a semi-transparent membrane exhibiting universal and quantized optical transmission [9]. This quantization fails for multilayer graphene thicker than a few layers, however the membrane retains a significant transparency up to a hundred layers [10].

1.2. Enhancing graphene coupling to photons by integration within an optical cavity

In all these previous studies, optical interference is at the origin of the visibility of graphene, and more generally gives a means to further optimize the interaction with incoming photons. Light–graphene coupling can indeed be further enhanced by integrating the graphene within an optical cavity. This has been recently achieved on photonic crystals [11] or in a Fabry–Perot cavity [12, 13]. It was shown that the sensitivity of graphene-based photon detectors [12–14] can be maximized in a cavity in which graphene is placed at resonant conditions. For example, thanks to the cavity effect, the absorbance of graphene in the THz range can exhibit a wavelength absorbance contrast reaching up to 70% modulation depth [14]. Recently, a suspended and movable graphene membrane has been integrated into a low-finesse optical cavity [15]. This demonstrates how light can be coupled to mechanical motion, and lead to active cooling of the graphene membrane, showing interesting prospects for the use of graphene for further optomechanical studies (cf figure 1). Similar cavity effects also apply to Raman scattered light. Raman spectroscopy, a powerful probe for graphene as it allows the local mapping of numerous physical parameters such as doping, structural defects, phonon temperature and mechanical stress, can be strongly affected by its coupling to a cavity. On this basis, interference enhancement of Raman scattering (IERS) has been studied for a long time [16] and more recently applied to graphene [17, 18] by tuning the SiO_2 thickness of samples made of supported or suspended graphene flakes. Similarly to what was achieved for elastically scattered light, IERS relies on the constructive interference of Raman scattered photons [16, 19]. Multiple wave interference in graphene over silica has been identified as a way to enhance the Raman signals, either coming from the graphene vibrations modes [18] or from adsorbates such as halogen species [17]. By varying the composition [20] and thickness [18] of the dielectric on which the graphene is deposited, modulation of the Raman lines has been shown.

In the present work, we show that, by building an optical micro-cavity made of self-supported multilayer graphene cantilever freestanding over silicon, interference phenomena occur not only in the back-reflected light but also in the Raman signals, coming either from graphene, from the silicon substrate or from any foreign adsorbed element. By electrostatic actuation of the graphene membrane, a time modulation synchronized with the application of an AC signal on the metallic electrodes can be achieved, offering a versatile platform for Raman studies.
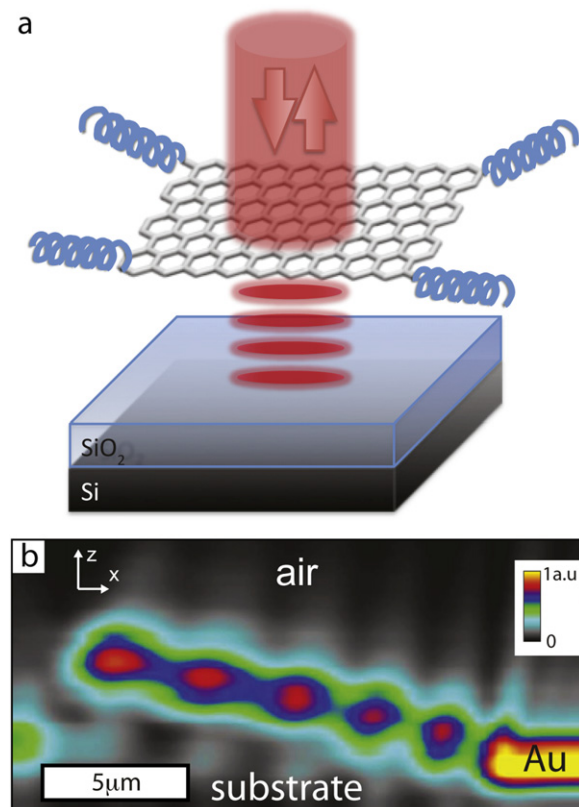

Figure 1. Graphene-based optomechanical systems. (a) A mechanically flexible and semi-transparent graphene-based membrane is freestanding over a silicon back mirror, constituting an optical cavity. Elastically and inelastically backscattered light is measured and gives indications on both the cavity thickness and the photonic interactions with the bottom and top mirrors. (b) Spatially resolved reflectance map acquired with a conical microscope in the cross-sectional (*X*, *Z*) plane at 532 nm for one typical sample. This experiment has been performed using scanning confocal microscopy at different focus points, showing the reflected intensity modulation due to optical interference within the cavity.

2. Fabrication and implementation of multilayered graphene electrically actuated optical cavities

Our system takes advantage of the outstanding optical, mechanical and electrical properties of graphene. Multilayers of typically 10–100 layers act as suspended semi-transparent mirror cantilevers, stiff enough to remain self-supported over more than 10 μm and electrically conducting to be actuated by an external electrostatic potential. The simultaneous high rigidity of this material and its semi-transparency allow the creation of an overhanging cantilever which is at the same time, light, rigid and semi-transparent (typically ∼25% transparency, ∼30% reflectance, ∼45% absorbance for 100 monolayers of graphene [10]). The batch integration of this system can be made using exfoliation of graphite on oxidized silicon, followed by lithography/deposition of electrodes and under etching (see methods for details (available at stacks.iop. org/JOpt/15/114010/mmedia)).

This optical micro-cavity defines an air wedge structure as shown in figure 2. Unlike conventional [21] graphene-based optical cavities with fixed geometries, the optical length
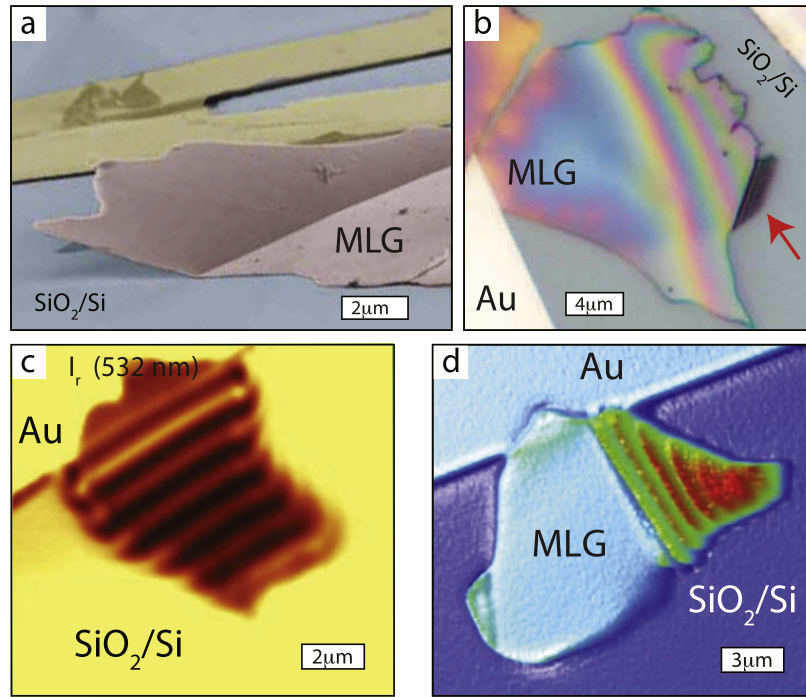
Figure 2. Multilayer graphene optical cavities. (a) Scanning electron micrograph of a multilayer graphene flake overhanging the silicon oxide defining an air wedge optical cavity. (b) Top view optical micrograph under white light illumination, showing iridescence. (c) Reflectance confocal (X, Y) map obtained by scanning a 532 nm laser probe, showing the equal thickness interference fringes. (d) Phase micrography recorded with an optical profilometer, revealing the interference pattern along the wedged membrane.

of this cavity increases linearly along the cantilever, which allows the observation of multiple interference fringes (cf figure 1). These equal thickness interference fringes, so-called Fizeau fringes, will be first described for reflected light and Raman scattering. Furthermore, we demonstrate the possibility to tune this optical cavity with a voltage applied to graphene, allowing us to control the wedge angle and thus the interference pattern. The resulting shift in the interference pattern can be used as an intensity modulation for a fixed laser probe, which in turn can be used to modulate the intensity of Raman signals. Taking advantage of the variable interference enhancement of Raman scattering, combined with the ability of graphene to be an excellent substrate for Raman scattering, we show the possibility to use this cavity as a tunable platform for molecular detection. Recently, our team has shown that similar suspended graphitic membranes can be used to simultaneously detect motion and stress [22] within the actuated cantilever using the stress-dependence of the Raman response. Prospects for the use of this novel family of systems for building hybrid platforms for Raman studies will be presented.

3. Optical Fizeau interference in the micro-cavity

3.1. Interferences in reflection

Optical interference fringes are observed along this air wedge device (cf figures 2(b)–(d) and 1(b)). As the local cavity thickness $h(\rho)$ (which corresponds to the vertical gap between the MLG membrane and the reflecting substrate) is

increased by $\delta h = \lambda/(2n_0)$, where λ and n_0 are respectively the wavelength and the optical index of air or vacuum (cf figure 3), a new interference maximum appears within the cavity. In figures 2(b) and (c), iridescence is observed under white light illumination and the interference pattern is measured at 532 nm. The wedge geometry implies that all points at equal distances from the hinge have equal light wave dephasing, forming a set of parallel Fizeau fringes (or equal thickness fringes). Note that the interference order $2h/\lambda$ is close to unity, as the thickness of the wedge is a mere $\lambda/2$, especially near the hinge position. In addition, for small wedge angles ($\alpha \sim 10°$), the in-plane distance between two adjacent fringes would be large enough to spatially resolve them by confocal microscopy imaging. By confocal imaging, AFM and profilometry measurements, we check that the geometry of the MLG cantilever is flat. This ensures that the gap between the MLG cantilever and the silicon substrate increases linearly from the hinge to the end of the cantilever. One can simply consider that the light beam enters the cavity and gets trapped for a certain number of reflections on both sides before escaping. For a high-finesse cavity, this trapping becomes efficient and the light field can be locally strongly enhanced inside the cavity. In our case, the wedged cavities (finesse ~ 10) do not exhibit the high-finesse characteristic of Fabry–Perot fringes: (i) because of the non-parallel wedge geometry, which causes wave detrapping at higher interference orders [23], and (ii) because the light absorption limit is not negligible in both the substrate and MLG membrane. The first argument, previously discussed by Brossel [24], can be interpreted in terms of
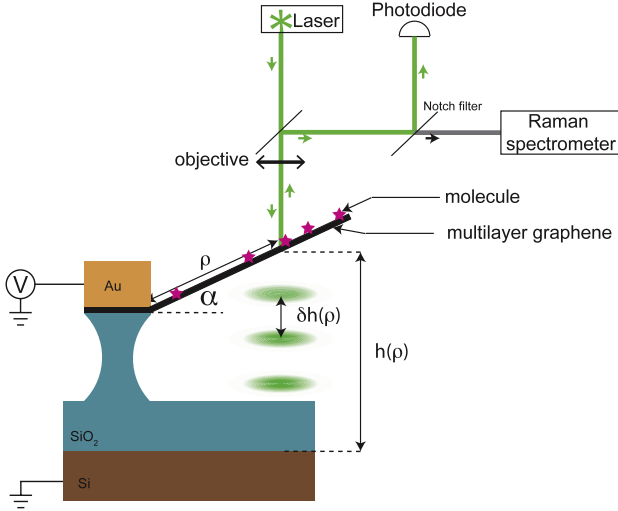
Figure 3. Schematics of the measurement setup. A multilayer graphene cantilever clamped between a silica pillar and a gold electrode is addressed by a gate voltage that controls its wedge angle α, which is probed by reflectometry (signal measured with a high bandwidth photodiode) and Raman spectrometry (filtered inelastic scattering signal measured with a spectrometer coupled to a CCD device). The height between two successive fringes in reflection is labeled $\delta h = \lambda/(2n_0)$. Raman-active molecular species (red stars) adsorbed on the mirror can be detected as well.

Figure 4. Spatial modulation of intensity of both reflected and Raman lines. Measurement of the interfringe width (averaged over the sample) as a function of the effective photon wavelength. Experimental data (•) are in agreement with a basic interferometric simulation (○) performed with Nanocalc, and follow a quasi-linear dispersion (dashed line), as suggested by equation (4). Points at 532 and 633 nm correspond to the light reflection for the two excitations, while the MLG Raman bands are labeled as G, 2D and 2D′, with the associated pump laser in brackets.

geometrical optics. Reflections of the multiply-reflected beam in the cavity are progressively shifted along the membrane, eventually escaping the cavity. Therefore, after a number p of reflections given by the Brossel criterion $p \leq \left(3\lambda/(8h\alpha^3)\right)^{1/3}$, the transmitted beam cannot be collected by the microscope objective. Such effect implies: (i) a low intensity of the interference fringe, (ii) an increase of its width along the membrane, (iii) a shift of the fringe along the wedge structure and (iv) an asymmetry in the fringe profile. The second reason why these cavities do not exhibit very high finesse is the strong absorption of light, which limits the reflected intensity $I_{\text{reflected}}$. Interestingly, the derivation of the reflected light in such an asymmetric cavity becomes a highly non-trivial problem when absorption effects have to be considered, as highlighted by Holden [25]. According to these two effects, one may derive the reflected light intensity:

$$I_{\text{reflected}}[\rho] \sim I^0 \left[\frac{\mathcal{F}}{2\mathcal{A}} (1 + \cos\phi_{\text{laser}}[\rho]) + \Gamma \right], \qquad (1)$$

where $I^0, \rho, \mathcal{F}, \mathcal{A}, \phi_{\text{laser}}[\rho]$ and Γ are respectively the incident laser light intensity, the laser position along the membrane, the cavity finesse, the absorption coefficient, the phase difference between two reflected beams, and a constant that depends slightly on the reflection coefficient [25]. One can express the phase difference $\phi_{\text{laser}}[\rho] = \frac{2\pi}{i_{\text{laser}}}\rho$ as a function of the interfringe i_{laser}, which is the distance separating two successive Fizeau fringes along the MLG membrane.

The Raman effect is an inelastic scattering process of light and gives information on the atomic displacements inside a material. Analysis of the probed optical phonons
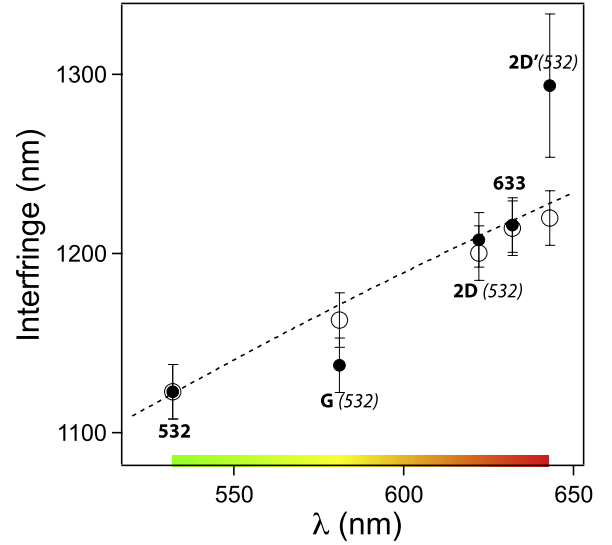
leads to a rich variety of intrinsic properties (thermal, mechanical, electronic, vibrational, structural) [3, 18, 22, 26, 27]. Moreover, since the Raman signal is related to the microscopic structure of matter, it is a fingerprint of many chemicals and molecules. The Raman fingerprint of the graphitic nano-system is made of two major G and 2D bands [26].

Interference patterns observed along MLG cavities from the reflection of the pump laser are also observed from the Raman scattered light and follow a similar behavior (see figures 5 and 4). Thus, one can see a situation where light sources are now localized on one side of the cavity (either the Si or MLG side). The light sources create Raman photons, which can enter the cavity and produce an interference pattern or get collected directly by the objective. Interestingly, not all the collected Raman photons contribute to the interference effect, since the collection angle is very large (NA = 0.95), and thus the collected Raman light has two contributions: (i) interference enhanced Raman (IERS) and (ii) standard Raman. Equation (1) is then modified, and we define I_{Raman} as the Raman intensity (i.e. the G band) measured along the membrane:

$$I_{\text{Raman}}[\rho] = I^0_{\text{Raman}}[\rho]$$
$$\times \left\{ \frac{\Omega_1}{4\pi} + \frac{\Omega_2}{4\pi} \left[\frac{\mathcal{F}}{2} \left(1 - \cos\phi^0_{\text{Ra}}[\rho] \right) \right] \right\} \qquad (2)$$

where $I^0_{\text{Raman}}[\rho]$ is the total Raman scattered intensity at position ρ and for a given laser power, without taking into account interference effects. $\Omega_1 = 2\pi \left(1 - \cos(\sin^{-1}\text{NA}) \right)$ is the solid collection angle for photons without the interference
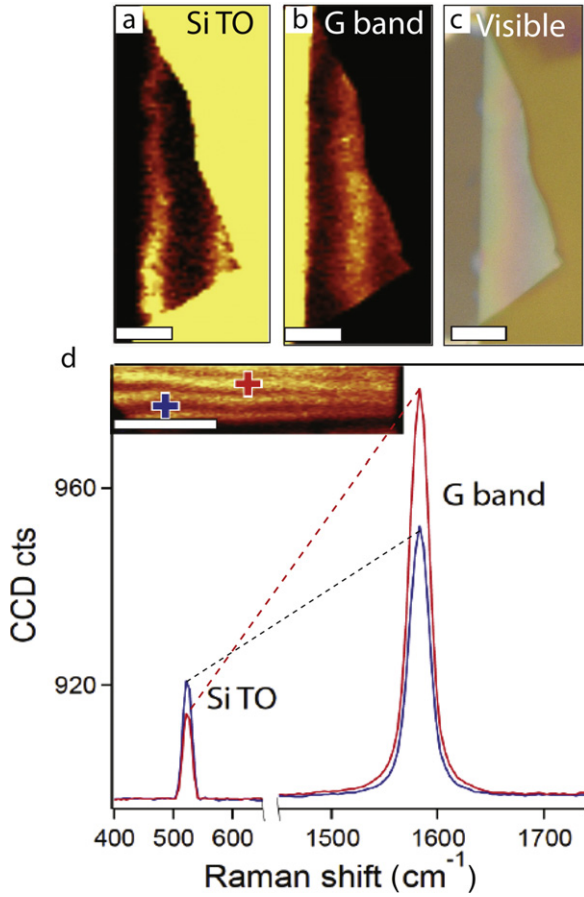
Figure 5. Multilayer graphene wedge structure overhanging silicon oxide. (a)–(c) Raman intensity maps of the silicon representative mode (Si-TO) and the G band are presented as well as the optical image of the corresponding device. Each mode presents its own interference pattern, which is clearly shifted due to chromatic dispersion within the cavity. (d) Raman spectra showing Si-TO and G bands taken at two different locations along the suspended MLG cantilever. The red curve is taken at a bright fringe of the G band intensity pattern, while the blue curve is taken at a dark fringe position. Inset: G band intensity profile with positions where the two spectra are taken. Scale bars represent 10 μm. The dotted lines join the two peaks of the same spectrum and show that their relative intensity is inversed when going from a bright to a dark fringe.

contribution, and Ω_2 is the solid collection angle for photons interfering in the cavity. $\phi_{Ra}^0[\rho] = \frac{2\pi}{i_{Ra}^0}\rho$ is the phase difference between interfering beams and i_{Ra}^0 is the theoretical interfringe for a given Raman mode in case of a homogeneous laser power. For isotropic scattering, the first term in equation (2) is independent of the position along the membrane and depends only on the numerical aperture. In our case, $\Omega_1/4\pi \sim$ 34%. The IERS signal (collection solid angle $\Omega_2 = 2\pi(1 - \cos\theta_2)$) obeying the Brossel criterion can be understood as the maximal interference order allowed for a light beam transmitted out of the cavity at a position laterally shifted by a distance smaller than the laser spot size. A limit angle $\theta_2 = \tan^{-1}[\lambda_{ph}/(4h[\rho])]$ is derived for two-wave interference. Thus, Ω_2 depends on the air wedge thickness $h[\rho]$: close to the hinge, Ω_2 can correspond to 1/3 of Ω_1 ($h[0] \sim 180$ nm, $\alpha \sim 12°$).

So far, we have introduced the intensity modulation for laser light (cf equation (1)) and for Raman scattered light (cf equation (2)). In equation (2), we have introduced the term $I_{Raman}^0[\rho]$, which depends on the laser position along the membrane, since we take into account a realistic case where the Raman scattered light intensity is affected by the modulation of the laser excitation intensity. This leads to:

$$I_{Raman}[\rho] = \frac{\mathcal{F}I_{Raman}^0}{8\pi}\left\{\Omega_1\left[1 - \cos\left(\frac{2\pi}{i_{laser}}\rho\right)\right]\right.$$
$$+ \frac{\Omega_2\mathcal{F}}{2}\left[1 - \cos\left(\frac{2\pi}{i_{laser}}\rho\right)\right]$$
$$\left.\times\left[1 - \cos\left(\frac{2\pi}{i_{Raman}^0}\rho\right)\right]\right\}. \quad (3)$$

It is worth noting that equation (3) shows the non-trivial dependence of the observed Raman Fizeau interfringe i_{Raman}, since it is now clear that there is beating effect due to interferometric modulation of the laser excitation. Three interfringe expressions are present: the measured Raman interfringe i_{Raman}, the absolute Raman interfringe (supposing constant laser power along the membrane) $i_{Raman}^0 = \lambda_{Raman}/(2\alpha n_0)$, and the excitation laser interfringe $i_{laser}\lambda_{laser}/(2\alpha n_0)$. From equation (3), two regimes appear: (i) $\Omega_1 \gg \frac{\Omega_2\mathcal{F}}{2}$ (Raman interference effect negligible) leading to $i_{Raman} \sim i_{laser}$, and (ii) $\Omega_1 \ll \frac{\Omega_2\mathcal{F}}{2}$ (Raman interference effect dominant) leading to one physical solution:

$$(i_{Raman})^{-1} = \frac{1}{2}[(i_{Raman}^0)^{-1} + (i_{laser})^{-1}]$$
$$i_{Raman} = \frac{1}{\alpha n_0}\frac{\lambda_{Raman}\lambda_{laser}}{\lambda_{Raman} + \lambda_{laser}}. \quad (4)$$

This expression, plotted in figure 4, fits the experimental data and the simulated points using ellipsometry simulation software. In figure 4, we clearly see that $i_{Raman} \neq i_{laser}$ and depends on the Raman scattered light wavelength.

In figures 5(a)–(c), interference fringes are measured via spatially resolved Raman spectroscopy for silicon (TO) and MLG (G, 2D and 2D') Raman lines. By taking advantage of this periodic shift with respect to λ (typically ~100 nm), the I_G/I_{Si} ratio can be tuned by moving the probe position (see figure 5(d)), in order to optimize the spatial modulation and background contrast. Such a modulation (by moving the laser) allows one to tune the optical cavity to maximize one Raman peak relative to another, which could be of great use in high-resolution Raman spectroscopy. This effect is even more pronounced if the finesse of the optical cavity is high (as suggested by equation (3)) and offers the possibility of effective rejection of unwanted Raman signals (substrate, residues, etc). Another manner to modulate this Raman signal is to realize electrostatic modulation.

4. Electrostatic modulation of the optical micro-cavity

The optical cavity thickness can be adjusted by varying the angle α through electrostatic actuation of the cantilever (see
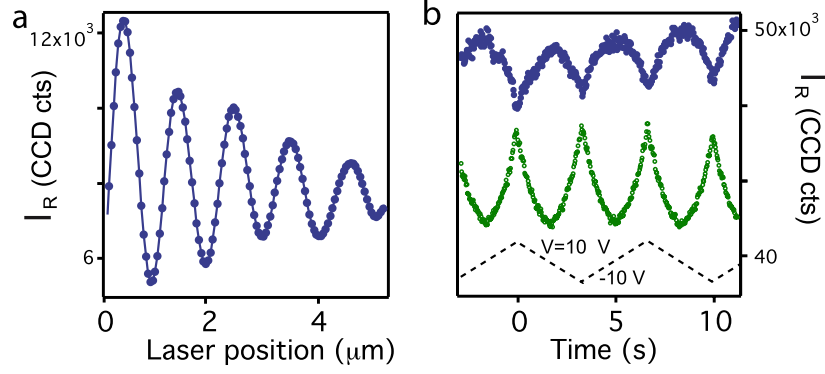
Figure 6. Spatial and time modulation of the back-reflected signals. (a) Reflected light intensity ($\lambda_{\text{laser}} = 532$ nm) along the MLG cantilever taken for a scan line perpendicular to the hinge. For each position of the laser, the elastic signal is measured using a photodiode. The laser position is swept using a piezoelectric scanning stage. Fizeau interference fringes clearly appear and one can finely tune the position of the laser to maximize the reflected or Raman signal. (b) Time modulation of the same reflected light intensity ($\lambda_{\text{laser}} = 532$ nm) at a fixed position while a triangular quasi-static potential (dashed line) is applied between the gate and the suspended membrane. The gate-modulated optical signal shows quadratic festoon-like behavior. As suggested by equation (7), the optical signal is modulated at twice the actuation frequency. Depending on where the laser is focused, the festoons are pointing up (laser focused at a rising edge of a fringe— ○) or pointing down (laser focused at a falling edge of a fringe— ●). Such a MLG cantilever offers the possibility to modulate either the elastic or inelastic backscattered optical signals both spatially and electrostatically.

figure 3), thus producing a shift in the interference pattern. This modulation of the cavity thickness $h(\rho)$ is achieved by applying a DC or AC voltage to the clamp electrode while the substrate is grounded. Thus $h(\rho, t) = h(\rho)_0 + \delta h(\rho, t)$, where $h(\rho)_0$ is the local cavity thickness or length at $V = 0$. This results in an attractive electrostatic force:

$$\vec{F} = -\frac{1}{2}\frac{\partial C_{\text{tot}}(h)}{\partial h}V^2\vec{u}_\theta = -B[h(\rho)_0]V^2\vec{u}_\theta. \quad (5)$$

This force (equation (5)) produces an angular deviation with respect to the equilibrium position. For driving frequencies $\Omega \ll \Omega_{\text{m}}$, where Ω_{m} is the mechanical resonant frequency (MHz range [22]), the motion of the cantilever of mass M is determined by linear response theory and $h(\rho, t)$ is then defined as the product of the mechanical susceptibility at low frequency $\chi_{\text{mac}} = M/\Omega_{\text{m}}^2$ and the applied force $F(t)$:

$$h(\rho, t) = \chi_{\text{mec}}F(t) = \chi_{\text{mec}}B[h(\rho)_0]V(t)^2. \quad (6)$$

It is worth noting when the laser spot is located 10 μm away from the hinge, the deviation $\delta h(\rho, t)$ does not significantly change the value of $B[h(\rho)_0]$ (<1%), which can be approximated as a constant.

We now implement interferometric detection of the motion, which would be maximum when the quantity $\chi_{\text{opt}} = \partial I_{\text{reflected,Raman}}/\partial h[\rho]$ is maximum, i.e. at a fringe edge. In our experiments, we manage to focus the laser beam at the fringe edge, and far away from the hinge, in order to get large motion amplitude. Therefore, it is legitimate that I_r is locally a linear function of $h(\rho, t)$, implying that for a small deflection $\delta h(\rho, t)$ the variation of reflected light intensity (or Raman scattered light) under electrostatic actuation could be written as follows:

$$\Delta I_{\text{reflected,Raman}}[\rho, t] \sim \chi_{\text{opt}}\chi_{\text{mec}}B[h(\rho)_0]V(t)^2. \quad (7)$$

Figure 6(b) shows the experimental values for reflected light intensity under a triangular electrostatic actuation. When we apply a potential which is a linear function of the

time, the associated change in the reflected light intensity will be quadratic in time, as suggested by the term in V^2 in equation (7). The alternation of parabolic sections and peculiar sharp points is therefore due to the kinks of the $V(t)$ function (triangular signal). We also observe that, depending on the laser spot position, festoon-like behavior points up or down. Actually, this is due to the sign of χ_{opt} (cf equation (7)), which changes sign from one side of the Fizeau fringe to the other (rising or falling edge). This effect allows us to calibrate precisely the magnitude of electrostatic actuation by analyzing the nonlinearities observed when more than one interfringe is swept (as shown in figure 8(b) and in [22]). As we have shown previously, the typical order of magnitude for quasi-static actuation is about 1 nm V^{-2} for $\rho \sim 10$ μm (thus, for 10 V, motion amplitude at 10 μm from the hinge is about 100 nm). By varying the gate voltage applied on the MLG, its angle can be adjusted over a wide range (giving a local thickness variation far exceeding the wavelength of the incoming light). Its motion can be actuated and followed in real time from DC up to the tens of MHz range (mechanical resonance). Examples of the optical detection of motion and stress of the membrane can be found in our previous work [22].

To summarize, by combining the observed optical Fizeau interference to the possibility of adjusting the cavity length by electrostatic actuation of the MLG cantilever, it is possible to tune the optical resonance of the optical wedged cavity. We now explore the potential of such interferometric enhancement with a graphene-based hybrid system to measure the Raman response of grafted molecules.

5. Graphene as a tunable Raman platform for molecular detection

5.1. Adsorbed species on graphene: hybrid graphene systems

One of the most promising aspects of graphene is the unique ability to combine its own properties with those
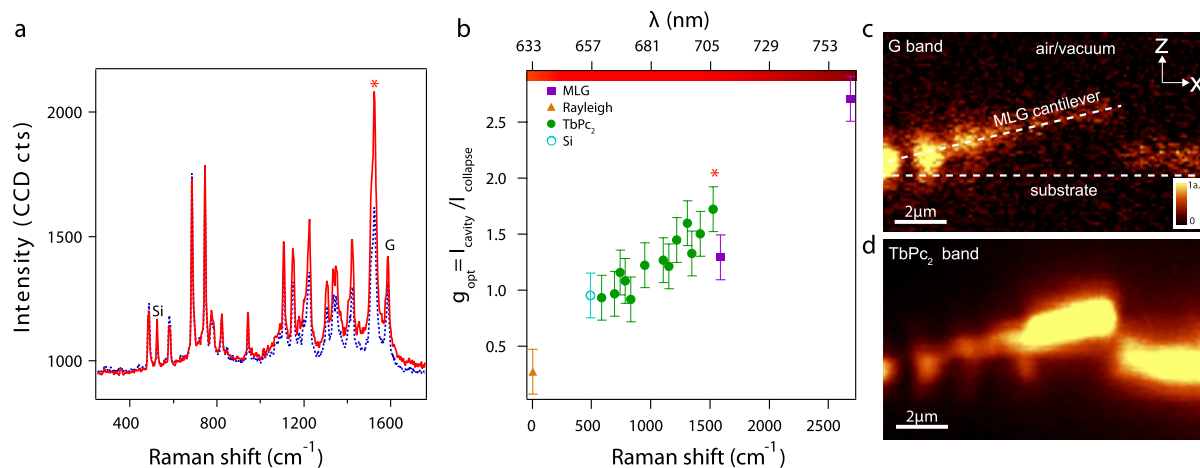
Figure 7. Modulation of Raman spectrum for generic adsorbed molecular species (a) Raman spectrum of a hybrid system composed of TbPc$_2$ molecules grafted on the MLG cantilever top mirror. The laser spot successively probes a bright fringe (red spectrum) for the MLG 2D band (red star) and onto the same system after mechanical collapse of the membrane on silicon (blue dotted spectrum). (b) Optical gain $g_{opt} = I_{cavity}/I_{collapsed}$ as a function of the wavelength of Raman scattered photons. From a practical point of view, each Raman mode g_{opt} is the ratio of the Raman intensity on top of the Fizeau fringe with respect to the Raman intensity on the collapsed cantilever. Raman modes of the MLG cantilever (■), substrate (○) and TbPc$_2$ (●) are represented, as well as the Rayleigh peak (▲). (c), (d) Raman mapping in the depth scan configuration (x, z) of the G band Raman intensity (c) and 1515 cm^{-1} TbPc$_2$ band (d) (indicated by ＊ in (a) and (b)). Fizeau fringes are clearly observed for the modes.

of a grafted species. Based on this feature, hybrid devices have been made to combine the electronic properties of graphene with the spin of a single molecular magnet [28]. Detection of single objects grafted on graphene still remains a crucial point to fully characterize hybrid devices and propose new ones. Recently, the idea of using graphene as a substrate for Raman signal enhancement has been proposed [27, 29], revealing that graphene has distinctive properties for Raman signal enhancement of grafted chemical species. The sensitivity can reach a very few molecules in number (∼10–100 for pyrene-substituted bis-phthalocyanine terbium TbPc$_2$ case) [27, 30] and is based on a chemical enhancement due to charge transfer between the graphene and the molecules. Graphene also has singular optical properties, making it a semi-transparent membrane in the visible range [9]. This property has been used to design optical cavities made of graphene membranes lying on transparent SiO$_2$ layer with a silicon back mirror [7]. Optical interference created by the cavity allows the detection of graphene flakes when the cavity thickness is adjusted to be in resonant conditions (i.e. maximizing the optical contrast). On that basis, interference enhancement of Raman scattering has been proposed [16–18] by tuning the SiO$_2$ thickness of samples made of supported or suspended graphene flakes parallel to the SiO$_2$/Si substrate. This phenomenon of interference enhancement of Raman scattering (IERS) relies on the constructive interference between Raman scattered photons [16, 19].

5.2. Cavity enhancement of molecules adsorbed on graphene

Raman spectra of this hybrid system, as shown in figure 7(a), indicates that the molecule is intact once deposited on the air wedge, which is consistent with our previous work [27].

Unlike the case where graphene is parallel to the plane of the substrate [27], our spatially resolved Raman mapping in the vertical plane (x, z) reveals Fizeau fringes for the TbPc$_2$ Raman bands in addition to the Raman signal corresponding to the multilayer graphene membrane (see figures 7(c) and (d)). By positioning the laser beam on the top of a bright interference Raman fringe of TbPc$_2$ (for example the Raman band at 1515 cm^{-1}), we measure an enhanced Raman signal of the molecule due to the interference effect. This enhancement depend on the finesse of the cavity, as suggested by equation (3), which is limited in our case by the absorbance of the two mirrors (silicon and graphene). A higher cavity finesse would increase the gain of the Raman lines and also offer the possibility, for instance, to completely extinguish a given Raman peak. In order to quantify the optical gain in our cavity, we measure the Raman spectrum on the same system for two different configurations: (figure 7(a)) respectively on a bright Fizeau fringe (red curve) and where the membrane is collapsed on the substrate (blue curve). In the second case, the optical thickness of the cavity is smaller than $\lambda/(2n_{SiO_2})$ for $\lambda \in [400; 800 \text{ nm}]$ ($h_{SiO_2} \sim 180 \text{ nm}$). The intensity ratio between the 2D peak on top of a Fizeau fringe (identified by a red star in figure 7(a)) and on the collapsed membrane is reported in figure 7(b). The optical gain for each of the Raman bands (molecule, silicon or membrane) follows an increasing dispersion behavior with the wavelength associated with each of the interference systems. Since the gain differs even within the set of Raman peaks, it becomes possible to preferentially enhance each Raman mode if one is able to change the thickness of the cavity by moving the laser or the membrane itself by electrostatic actuation, as we will see in section 5.3.

5.3. AC gate modulation of Raman lines of generic molecular species for molecular detection

As described previously, the Raman response of TbPc$_2$ molecules grafted on the suspended MLG membrane is affected by the interference phenomenon. By applying an AC voltage, the thickness of the cavity—and hence the position of TbPc$_2$ fringes—is periodically shifted (cf equation (7)). Adjusting the cavity length offers two features that are unique for generic Raman studies and potentially very useful to detect the tiny Raman signal emitted by a small amount of molecules: first the possibility to adjust the molecule under the laser probe up to a resonating position to maximize the Raman signal of the molecules. Second, the possibility to modulate the Raman intensities in a synchronized way with the AC voltage, a feature which potentially allows lock-in detection at a specific wavelength. To validate these two features, we have measured the response of the Raman spectra with respective applications of AC and DC voltages (figures 8(a) and (b), respectively).

For an applied AC sawtooth signal (figure 8(a)), we systematically detect a festoon-like response of the reflected light on the membrane, which is similar to what was observed for a graphene Raman signal, as shown in figure 6(b). When V_{AC} is gradually increased above $V_{AC} = 6$ V, the thickness of the cavity then spans $\delta h = \lambda/2n_0$, which means that one full Fizeau interference fringe has been passed through—explaining the dip which appears in figure 8(a). In figure 8(b), the Raman intensity of the TbPc$_2$ mode (1515 cm^{-1}) is plotted versus the applied voltage and the measured Raman signal is compared to a collapsed immobile membrane. The optical gain is maximum when the thickness of the cavity was adjusted to have a bright fringe (constructive interference) of the molecule Raman mode (for $V_{AC} > 7$ V). The optical cavity is thus modulated electrostatically to adjust its thickness, which maximizes the Raman line intensity. This important result allows synchronized detection methods where, for example, the excitation signal is locked with the recorded frequency of Raman spectrum. Such a technique would lower the detection threshold of adsorbed molecules on the membrane, leading towards the detection of a single object. Thanks to the electrostatic modulation of the cavity, one can select the Raman modes enhanced by constructive interference. By using this phenomenon, we can thus invert the intensity ratio between the selected modes and all other Raman signals. For example, we can selectively reject the fluorescence signal, thus improving the signal to noise ratio of the Raman spectra.

6. Conclusion

We have characterized the properties of simply clamped graphene cantilevers that act as a dual mechanical and optical resonators: both NEMS and Fabry–Perot-like cavities. This combination realizes an integration of a Raman based platform for the detection of molecular grafted species. When overhanging above oxidized silicon substrates, graphene cantilevers implement an optical cavity with a finesse in
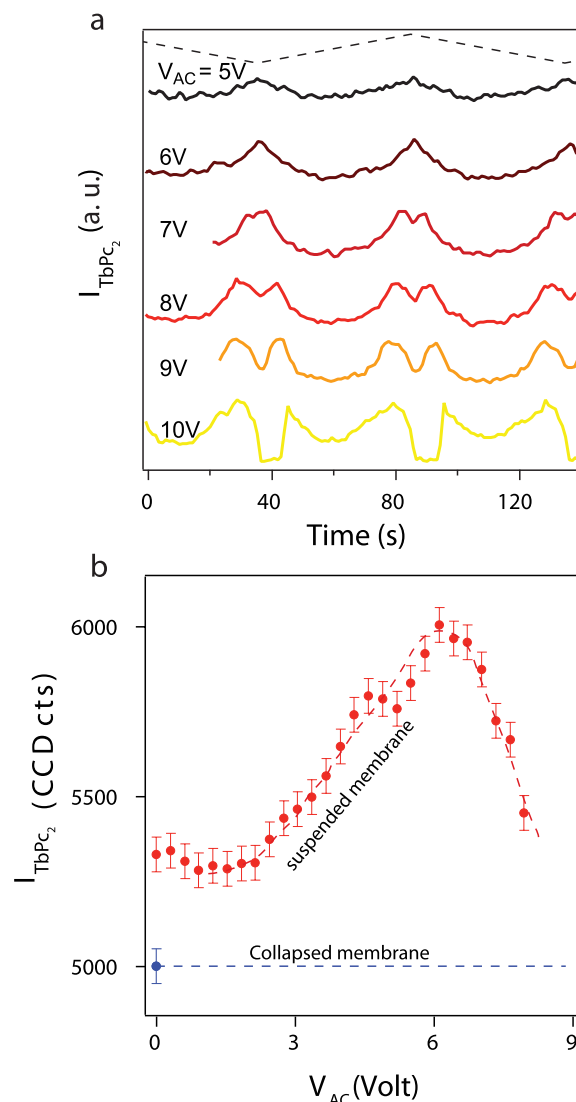

Figure 8. Time modulation and cavity enhancement of Raman lines of generic molecular species adsorbed on the graphene MLG. (a) Time trace of the 1515 cm^{-1} TbPc$_2$ Raman band while the MLG cantilever is electrostatically actuated with an external triangular potential δV_{AC} (dark dashed line). $I_{TbPc_2}(t)$ shows festoon-like behavior which is distorted as δV_{AC} becomes larger that 7 V. (b) Evolution of the same grafted molecule Raman signal I_{TbPc_2} as a function of the static actuation. Red dots are recorded for a suspended movable MLG cantilever, while blue dots refer to the same position after the MLG mirror has been collapsed. The cavity is in resonant conditions for $\delta V_{AC} \sim 6$ V for that particular Raman mode at 1515 cm^{-1}.

the range 5–10. Thickness variations within the air wedge between the graphene membrane and silica induce equal spacing fringes (Fizeau fringes) in the reflected and scattered light. We have shown that such an optical cavity exhibits optical interference patterns (Fizeau fringes), visible for both the incoming laser beam and Raman scattered photons. The fact that both elastic and inelastic scattering responses give rise to a series of interference patterns with specific signatures and interfringes, allowing splitting of each Raman mode coming from different chemical origins and vertical positions using this feature, we have, for example, been able to

selectively reject the graphene Raman signals from the silicon substrate. Such tuning is possible either by moving the laser spot along the Fizeau fringe pattern, or by electrostatically actuating the cavity. Moreover, it constitutes a case-study system to get a comprehensive picture of optical interference within graphene-based optical cavities. When the graphene surface is functionalized with π-stacked molecules, the Raman signal intensity is modulated by actuation of the cavity length with the gate voltage, and shows an enhancement which is maximum when the characteristic wavelength of the associated Raman band is at a resonant condition. The achieved time modulation of Raman signals paves the way for the lock-in type detection for single molecule Raman spectroscopy. The extension of that fine space and time tuning to any arbitrary Raman signal originating from chemicals grafted on the graphene shows that our original platform offers a promising device for highly sensitive Raman experiments on chemicals on graphene. Further works are underway to take advantage of this system for studies by Raman spectroscopy of single molecular systems.

Acknowledgments

References

[1] Takadoum J 2010 Black coatings: a review *Eur. Phys. J.-Appl. Phys.* **52** 7
[2] Kim K S, Zhao Y, Jang H, Lee S Y, Kim J M, Kim K S, Ahn J-H, Kim P, Choi J-Y and Hong B H 2009 Large-scale pattern growth of graphene films for stretchable transparent electrodes *Nature* **457** 706–10
[3] Cooper D *et al* 2012 Experimental review of graphene *ISRN Condens. Matter Phys.* **2012** 56
[4] Novoselov K S, Geim A K, Morozov S V, Jiang D, Zhang Y, Dubonos S V, Grigorieva I V and Firsov A A 2004 Electric field effect in atomically thin carbon films *Science* **306** 666
[5] Novoselov K S, Jiang D, Schedin F, Booth T J, Khotkevich V V, Morozov S V and Geim A K 2005 Two-dimensional atomic crystals *Proc. Natl Acad. Sci. USA* **102** 10451–3
[6] Zhang Y, Tan Y-W, Stormer H L and Kim P 2005 Experimental observation of the quantum Hall effect and Berry's phase in graphene *Nature* **438** 201–4
[7] Blake P, Hill E W, Castro Neto A H, Novoselov K S, Jiang D, Yang R, Booth T J and Geim A K 2007 Making graphene visible *Appl. Phys. Lett.* **91** 063124
[8] Roddaro S, Pingue P, Piazza V, Pellegrini V and Beltram F 2007 The optical visibility of graphene: interference colors of ultrathin graphite on SiO$_2$ *Nano Lett.* **7** 2707–10

[9] Nair R R, Blake P, Grigorenko A N, Novoselov K S, Booth T J, Stauber T, Peres N M R and Geim A K 2008 Fine structure constant defines visual transparency of graphene *Science* **320** 1308
[10] Skulason H, Gaskell P and Szkopek T 2010 Optical reflection and transmission properties of exfoliated graphite from a graphene monolayer to several hundred graphene layers *Nanotechnology* **21** 295709
[11] Gu T, Petrone N, McMillan J F, van der Zande A, Yu M, Lo G Q, Kwong D L, Hone J and Wong C W 2012 Regenerative oscillation and four-wave mixing in graphene optoelectronics *Nature Photon.* **6** 554–9
[12] Furchi M *et al* 2012 Microcavity-integrated graphene photodetector *Nano Lett.* **12** 2773–7
[13] Engel M, Steiner M, Lombardo A, Ferrari A C, Löhneysen H V, Avouris P and Krupke R 2012 Light–matter interaction in a microcavity-controlled graphene transistor *Nature Commun.* **3** 906
[14] Sensale-Rodriguez B *et al* 2012 Extraordinary control of terahertz beam reflectance in graphene electro-absorption modulators *Nano Lett.* **12** 4518–22
[15] Barton R A *et al* 2012 Photothermal self-oscillation and laser cooling of graphene optomechanical systems *Nano Lett.* **12** 4681–6
[16] Connell G A N, Nemanich R J and Tsai C C 1980 Interference enhanced Raman scattering from very thin absorbing films *Appl. Phys. Lett.* **36** 31
[17] Jung N, Crowther A C, Kim N, Kim P and Brus L 2010 Raman enhancement on graphene: adsorbed and intercalated molecular species *ACS Nano* **4** 7005–13
[18] Yoon D, Moon H, Son Y-W, Choi J, Park B, Cha Y, Kim Y and Cheong H 2009 Interference effect on Raman spectrum of graphene on SiO$_2$/Si *Phys. Rev.* B **80** 1–6
[19] Fainstein A, Jusserand B and Thierry-Mieg V 1995 Raman scattering enhancement by optical confinement in a semiconductor planar microcavity *Phys. Rev. Lett.* **75** 3764
[20] Castriota M, Cazzanelli E, Pacilè D, Papagno L, Girit Ç O, Meyer J C, Zettl A, Giarola M and Mariotto G 2010 Spatial dependence of Raman frequencies in ordered and disordered monolayer graphene *Proc. Diamond 2009, The 20th European Conf. on Diamond, Diamond-Like Materials, Carbon Nanotubes and Nitrides, Part 1; Diamond Relat. Mater.* **19** 608–13
[21] Ling X, Xie L, Fang Y, Xu H, Zhang H, Kong J, Dresselhaus M S, Zhang J and Liu Z 2010 Can graphene be used as a substrate for Raman enhancement? *Nano Lett.* **10** 553–61
[22] Reserbat-Plantey A, Marty L, Arcizet O, Bendiab N and Bouchiat V 2012 A local optical probe for measuring motion and stress in a nanoelectromechanical system *Nature Nanotechnol.* **7** 151–5
[23] Rogers J R 1982 Fringe shifts in multiple-beam Fizeau interferometry *J. Opt. Soc. Am.* **72** 638
[24] Brossel J 1947 Fabry Perot interferometer *Proc. Phys. Soc.* **59** 460–3
[25] Holden J 1949 Multiple-beam interferometry: intensity distribution in the reflected system *Proc. Phys. Soc.* B **62** 405
[26] Ferrari A C *et al* 2006 Raman spectrum of graphene and graphene layers *Phys. Rev. Lett.* **97** 1–4
[27] Lopes M *et al* 2010 Surface-enhanced Raman signal for terbium single-molecule magnets grafted on graphene *ACS Nano* **4** 7531–7
[28] Candini A, Klyatskaya S, Ruben M, Wernsdorfer W and Affronte M 2011 Graphene spintronic devices with molecular nanomagnets *Nano Lett.* **11** 2634–9
[29] Ling X and Zhang J 2010 Interference phenomenon in graphene-enhanced Raman scattering *J. Phys. Chem.* C **115** 2835–40
[30] Klyatskaya S, Mascarós J R G, Bogani L, Hennrich F, Kappes M, Wernsdorfer W and Ruben M 2009 Anchoring of rare-earth-based single-molecule magnets on single-walled carbon nanotubes *J. Am. Chem. Soc.* **131** 15143–51